Affinity of nicotinoids to a model nicotinic acetylcholine receptor (nAChR) binding pocket in the human brain

Garrett D. Santis,[†] Yuika Okura,[‡] Keisuke Hirata,[‡,¶] Shun-Ichi Ishiuchi,[‡,¶,§] Masaaki Fujii,[¶,§,‖] and Sotiris S Xantheas [*,†,¶,⊥]

†*Department of Chemistry, University of Washington, Seattle, Washington 98195, United States*

‡*Department of Chemistry, School of Science, Tokyo Intitute of Technology; 2-12-1 4259 Ookayama, Meguro-ku Tokyo, 152855, Japan*

¶*Tokyo Tech World Research Hub Initiative (WRHI), Institute of Innovation Research, Tokyo Institute of Technology; 4259 Nagatsuta-cho, Midori-ku, Yokohama, 226-8503, Japan*

§*Laboratory for Chemistry and Life Science, Institute of Innovative Research, Tokyo Institute of Technology; 4259 Nagatsuta-cho, Midori-ku, Yokohama, 226-8503, Japan*

‖*School of Life Science and Technology, Tokyo Institute of Technology; 4259 Nagatsuta-cho, Midori-ku, Yokohama, Kanagawa, 226-8503, Japan*

⊥*Advanced Computing, Mathematics and Data Division, Pacific Northwest National Laboratory, 902 Battelle Boulevard, P.O. Box 999, MS K1-83, Richland, Washington 99352, United States*

E-mail: sotiris.xantheas@pnnl.gov

Abstract

The binding affinity of nicotinoids to the binding residues of the $\alpha_4\beta_2$ variant of the nicotinic acetylcholine receptor (nAChR) was identified as a strong predictor of the nicotinoid's addictive character. Using *ab-iniito* calculations for model binding pockets of increasing size comprising of 3, 6, and 14 amino acids (3AA, 6AA, and 14AA) that are derived from the crystal structure, the differences in binding affinity of 6 nicotinoids, namely nicotine (NIC), nornicotine (NOR), anabasine (ANB), anatabine (ANT), myosmine (MYO), and cotinine (COT) were correlated to their previously reported doses required for increases in intracranial self-stimulation (ICSS) thresholds, a metric for addictive characteristics. By employing the many body decomposition, differences in the binding affinities of the various nicotinoids could be attributed mainly to the proton exchange energy between the Pyridine and *non*-Pyridine rings of the nicotinoids and the interactions between them and a handful of proximal amino acids, namely Typ156, Typβ57, Tyr100, and Tyr204. Interactions between the guest nicotinoid and the amino acids of the binding pocket were found to be mainly classical in nature, except for those between the nicotinoid and Typ156. The larger pockets were found to model binding structures more accurately and predicted the addictive character of all nicotinoids. Smaller models, which are more computationally feasible, would only predict the addictive character of nicotinoids similar to that of nicotine. The present study identifies the binding affinity of the guest nicotinoid to the host binding pocket as a strong descriptor of the nicotinoid's addiction potential and as such it can be employed as a fast screening technique for the potential addiction of nicotine analogs.

I. Introduction

Nicotine addiction is a global health crisis and has been perpetuated by the evaluation of tobacco products in response to social and regulatory shifts.[1–3] Recently, nicotine consumption through flavored vape products has revitalized tobacco use in the youngest generation.[4,5] In response, the US Food and Drug Administration (FDA) is taking regulatory action, announc-

ing the plan to limit the amount of nicotine in all products.[6] Just this past year, the FDA announced that it would lower the amount of nicotine allowed in cigarettes "to minimally addictive or non-addictive levels."[7] The tobacco industry has a mandate to lower the amount of nicotine in their products and the incentive to introduce nicotine-like analogues (nicotinoids) to their products to abide by the upcoming regulations. Understanding the mechanism of nicotine addiction from a molecular level and predicting how similar molecules will act in this capacity is therefore of great importance in the tobacco industry and tobacco regulation.

The biochemical mechanism for nicotine addiction is well understood. Nicotine and similar alkaloids (nicotinoids) are known to interact with a family of neuroreceptors known as nicotinic acetylcholine receptors (nAChR).[2,8–10] These receptors are found throughout the muscular and nervous systems with roles in diseases ranging from Alzheimer's, schizophrenia, and addiction.[2,8,11–13] Each receptor is a pentameric ion channel consisting of various subunits, α-ϵ.[14] Receptors in the central nervous system, including the one responsible for addiction and pleasure, consist of only α and β subunits. Agonists bind to one side of each α subunit, which opens the ion-gate that causes intracellular signaling and eventual dopamine release.[10,15] Antagonists are also known to bind without opening the ion channel.

Nicotine is known to be most selective to the specific nAChR $\alpha_4\beta_2$ variant, found in the central nervous system and tied to the pleasure response.[2,16–21] It is through this interaction that nicotine is addictive. Crystal structures of nAChR and similar acetylcholine binding proteins (AChBP) show that nicotine binds at the interface between the α and β strands through strong interactions between the pyrrolidine nitrogen and the tryptophan residue.[16,17,20,21] It is assumed that nicotine remains protonated at the pyrrolidine nitrogen due to the nature of the interaction. The energetics of the protonation of nicotine have been the focus of previous studies.[22–24] With two basic nitrogen atoms, two singly-protonated isomers (protomers) are possible, namely the pyridine protomer (Pyri-H^+) and the pyrrolidine protomer (Pyrro-H^+). It is known that at biological pH, nicotine and similar compounds exist as Pyrro-H^+.[25–27] Recent studies, however, show that a nearly equal mixture of the

two nicotine protomers is present in the gas phase, whereas Pyri-H^+ dominates in the gas phase nornicotine, the demethylated form of nicotine.[22,28] Therefore, the stability of both protonation sites in non-aqueous environments, such as the gas phase and peptide pockets, is an important consideration, despite the strong evidence that a single protomer is present in biological systems.

This work focuses on quantifying and analyzing the nature of the interactions between nicotinoids and the nAChR $\alpha_4\beta_2$ receptor in an effort to correlate the binding affinity to the level of addiction. The addictive thresholds of nicotine and other similar nicotinoids have been previously reported through intercranial self-stimulation (ICSS) threshold studies.[3] These studies examined 6 nicotinoids found naturally in tobacco leaves, viz. nicotine (NIC), nornicotine (NOR), anabasine (ANB), anatabine (ANT), myosmine (MYO), and cotinine (COT), with the results displayed in Figure 1 together with the structures of their bioactive protonated forms. The neutral (not protonated) forms of these compounds are composed of two heterocyclic rings that contain four or five carbon atoms and one nitrogen atom each. Specifically, they all have a common basic 6-membered pyridine ring (located at the top right of each structure in Figure 1) that is structurally related to benzene, with one methine group (=CH–) replaced by a nitrogen atom, and differ in the second heterocyclic ring, which is either 5- or 6-membered (located at the bottom left of each structure in Figure 1), as follows: NIC and NOR have pyrrolidine, a 5-membered cyclic amine containing four carbon and one nitrogen atoms that is methylated in NIC (N-methyl-pyrrolidine). ANB has piperidine, a 6-membered heterocyclic amine containing five methylene (–CH_2–) bonds and one amine bridge (–NH–). MYO has 1-pyrroline, a cyclic 5-membered imine with the double bond next to the nitrogen atom. ANT has 3-piperideine, a 6-membered ring with five carbon atoms, one nitrogen atom, and a double bond. Finally, COT has N-methyl-2-piperidone, which is a 5-membered lactam. The protonation of these nicotinoids can occur either on the pyridine nitrogen (Pyri-H^+ protomer) – a common protomer for all 6 nicotinoids since they all have a pyridine ring – or on the nitrogen atom of the other-than-pyridine ring. Since this second

ring is different for the various nicotinoids, we will hereafter refer to that second protomer as the *non*-Pyri-H^+ one (note that this protomer corresponds to the bioactive form and it is the one shown for all nicotinoids in the right panel of Figure 1). The left panel of figure 1 is composed using the raw data in Figure 1 of reference[3] that was provided by one of the authors of that study. In the rodant model, it is found that NIC is the most addictive naturally occurring nicotinoid, NOR and ANB are less addictive, MYO and ANT could be marginally addictive, and COT is virtually non-addictive.[3] These ICSS studies provide an indispensible benchmark that quantifies the potency of these six nicotinoids to elicit addictive behaviors.

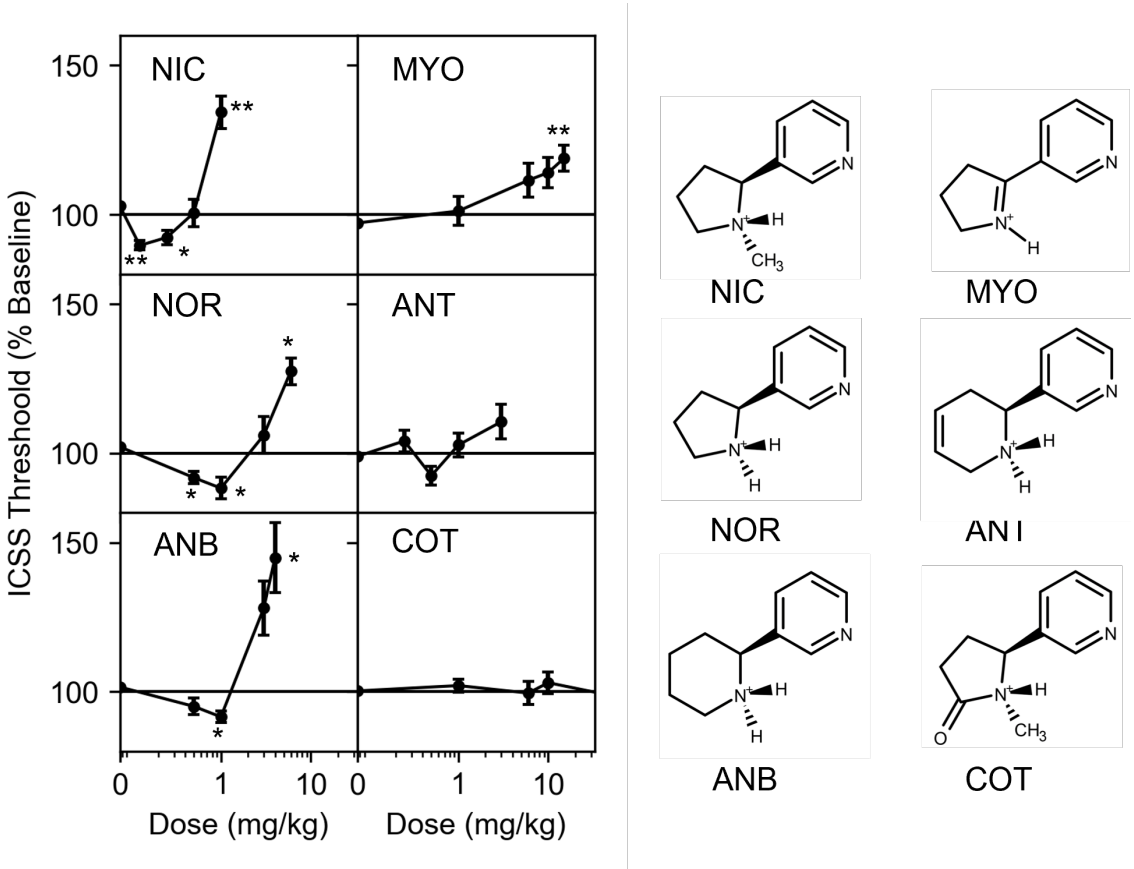

Figure 1: The six nicotinoids that have been studied through ICSS threshold experiments by Harris *et. al.*,[3] reproduced with their permission. Stars (*) represent p-values < 0.05 and double stars (**) p-values < 0.01, describing the probability that the population at that dose level is different than the baseline.

We computed the interaction between models of the nAChR $\alpha_4\beta_2$ binding pocket (p) and

the 6 nicotinoids (X) from ab-initio calculations. These models were built with progressively increasing sizes with the objective of incorporating the relevant interactions between the nicotinoids and the environment of the binding pocket. Our intent was to investigate whether the binding affinity of nicotinoids correlates with their reported ICSS threshold increasing/decreasing doses,[3] in other words whether the binding energy to the pocket is a potential descriptor for addictiveness that can be used for the fast and efficient screening of future nicotine analogs. Additionally, the various energetic components of the total binding were analyzed in an effort to provide insight into predicting the binding affinity from molecular properties of the various pieces comprising the binding pocket and to develop a computationally efficient protocol for predicting addiction.

II. Methodology

The electronic structure calculations were performed at the ωB97X-D[29]/6-31++G(d,p)[30,31] Density Functional level of theory[32] using Gaussian 16.[33] To speed up the optimization process, geometries were pre-optimized with the smaller 3-21+G basis set,[34,35] and then refined with the larger 6-31++G(d,p) set. The PCM solvent model was used to describe the fully solvated state of each nicotinoid for comparisons to more biologically relevant energy differences.[36] The ωB97X-D functional was chosen for its ability to describe long-range interactions ranging from hydrogen bonding to π-type interactions,[29,37,38] whereas the 6-31++G(d,p) basis set was chosen as a compromise between efficiency and accuracy, viz. minimizing the computational cost while including diffuse and polarization functions.

We constructed three models for the binding pocket based on the reported positions of the heavy atoms of the $\alpha_4\beta_2$ nAChR.[20] Amino acids were selected from the crystal structure of the human $\alpha_2\beta_4$ nAChR (PDB 5KXI).[39] This structure was chosen over the more recently reported structure by Walsh et.al.[21] due to the potential effects that antibodies could induce on the local geometry in the latter study. The model pockets were built by selecting amino

acids deemed to be important for the interaction with the nicotinioids. The C-terminus was capped with a terminal amide whereas the N-terminus was capped with a neutral amine to model the interactions of each functional group while minimizing the model size and computational cost. The hydrogen atoms were subsequently added using chemical intuition. The nitrogen and carbon atoms in the backbone of each model pocket were held rigid to maintain the structure of the ligand-bound receptor and ion channel reported in the desensitized state.[20] Side chains and hydrogen atoms were allowed to relax. These model pockets were constructed to capture specific interactions between the nicotinoid and the pocket (Figure 2). The smallest model (3AA) consisted of the three closest amino acids and captured the direct molecular orbital and hydrogen bonding interactions (Trp156, Thr157, and Trpβ57). The next model (6AA) added the Asp96 residue and two hydrogen bonding amino acids (Ser155 and Tyr158) for a total of 6 amino acids to model the electrostatics of the binding pocket and to increase nucleophilicity. Finally, to capture steric effects, the largest model (14AA) added 8 more free amino acid residues (Tyr100, Tyr197, Cys199, Cys200, Tyr204, Serβ108, Leuβ121, and Proβ123) whose side chains constrain the nicotinoids in the pocket (total of 14 amino acids). The total number of basis functions used in the geometry optimizations of the model pockets with the 6-31++G(d,p) basis set were 901 (3AA), 1540 (6AA), and 3466 (14AA), respectively. The number of basis functions increases by up to 325 basis functions upon the inclusion of the nicotinoids to the respective model pockets. The largest calculations involved geometry optimizations for the COT-14AA combined nicotinoid-pocket system with 3791 basis functions with 726 unconstrained nuclear degrees of freedom.

The addictive thresholds previously reported by ICSS studies in a rat model[3] are statistical measurements that were translated to single values for the analysis of this work. Two important values are chosen from the experiments, namely (i) the ICSS threshold-decreasing dosages, where the ICSS threshold falls statistically below the baseline, and (ii) an ICSS threshold-increasing dosage where the ICSS threshold jumps statistically above the baseline. The ICSS threshold-decreasing dosage is selected to be 0.125, 0.5, and 1.0 mg/kg for NIC,

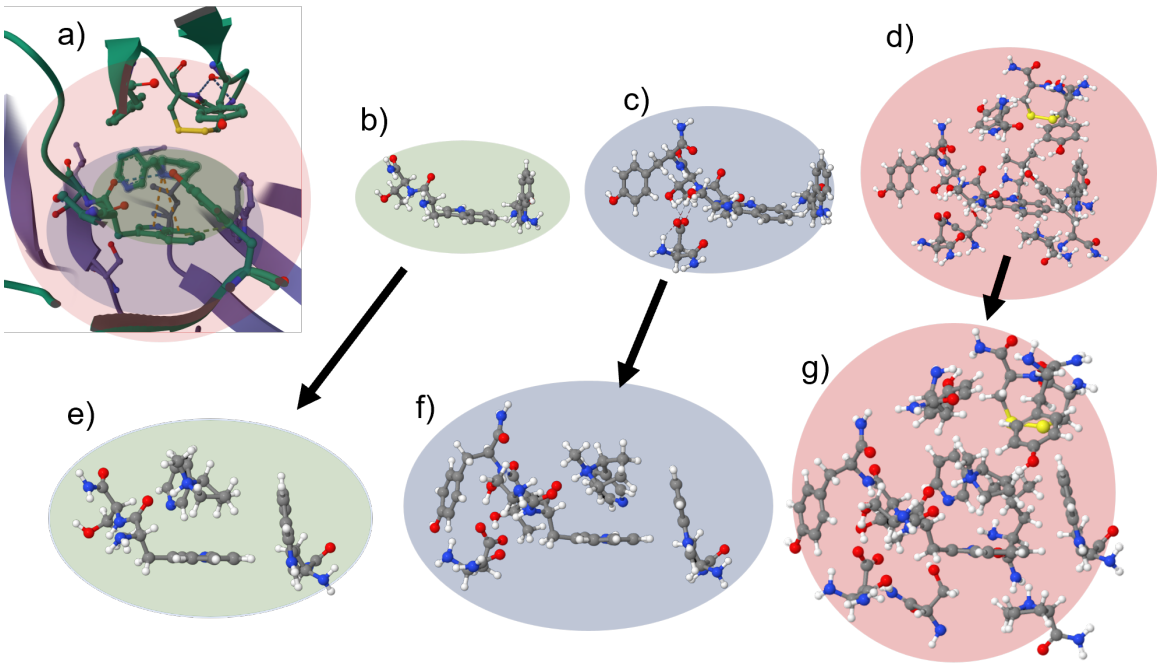

Figure 2: Model pockets were constructed from the crystal structure reported in PDB 5KXI.[39] (a) the binding domain. The three model pockets containing (b) 3, (c) 6 and (d) 14 amino acids used in this study. (e)-(g) nicotine bound to the three model pockets. The TYP100 residue is removed from (g) to more easily see nicotine.

NOR, and ANB. The ICSS threshold-increasing dosage is selected to be 1.0, 6.0, 3.0, and 15.0 mg/kg for NIC, NOR, ANB, and MYO respectively. These values were chosen as the lowest dosage, which results in p values less than 0.05 and the ICSS threshold is below or above the baseline. Both metrics are important to describe the potential addictive character of nicotinoids, since the ICSS decrease is associated with the abuse potential, whereas the ICSS increase is associated with withdrawal.[40] ANT and COT were not assigned addictive values because no measured dosages elicited ICSS thresholds statistically different from the baseline. It should be noted that COT is considered completely non-addictive (threshold dosage >100 mg/kg), whereas ANT may still be addictive outside the range of the dosages tested.[3]

The binding energies reported in this work were considered in the gas phase because the constructed model pockets do not include amino acid residues that could shield the bound ligand from solvent interactions. The binding energies of the nicotinoids to the respective

pocket were computed and analyzed following the scheme shown in Figure 3. Specifically, the total binding energy of nicotinoid X in pocket p_i, $\Delta E(X, p_i)$, is

$$\Delta E(X, p_i) = E_{\mathrm{X}}^{p_{\mathrm{i}}} - [E_0^{p_{\mathrm{i}}} + E_{\mathrm{X}}] \tag{1}$$

where subscripts "0" and "X" indicate an empty and filled (with nicotinoid X) pocket, respectively, $E_X^{p_i}$ is the energy of the optimized pocket with the nicotinoid X=NIC, NOR, ANB, ANT, MYO, COT, $E_0^{p_i}$ is the energy of the constrained and optimized (empty) pocket p_i=3AA, 6AA, 14AA, and E_0^X is the energy of the most stable gas phase protomer of nicotinoid. All relative energies are reported with respect to NIC.

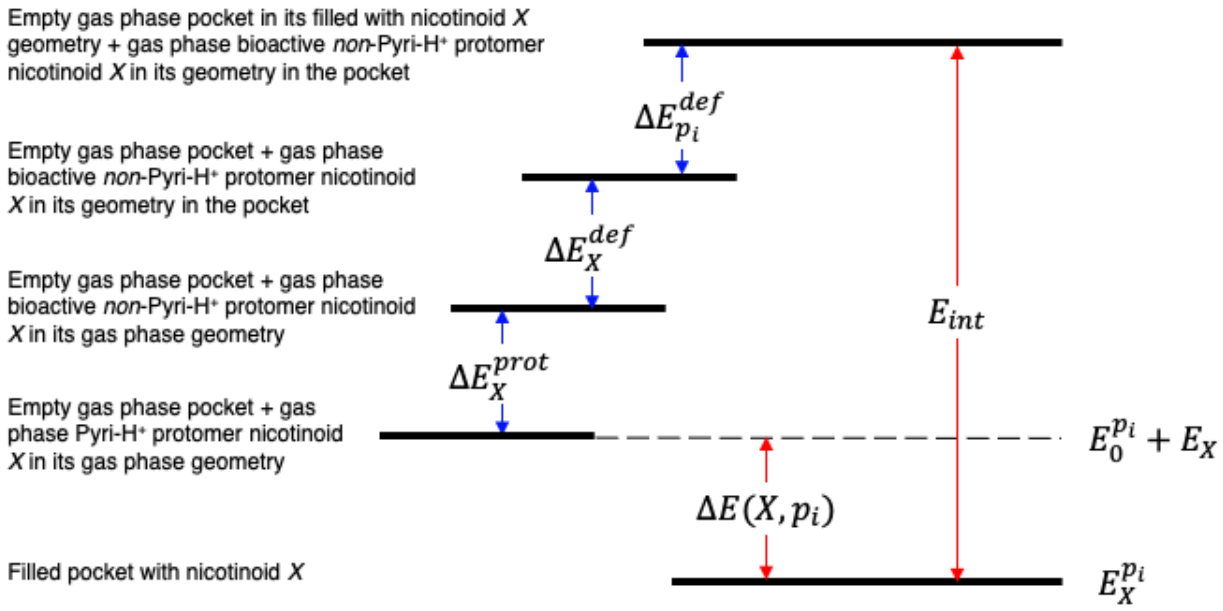

Figure 3: Definition of the various components of the binding energy, eqs. 1 and 2. Blue/red arrows indicate positive/negative energies. The dashed line indicates the reference of zero energy.

Following the scheme shown in Figure 3 the process of inserting nicotinoid X in the pocket can be thought of proceeding via the following steps: (i) nicotinoid X is promoted from the most stable gas phase structure (Pyri-H$^+$ except for MYO for which the *non*-Pyri-H$^+$ protomer is lowest in energy) to its bioactive *non*-Pyri-H$^+$ (Pyri-H$^+$ for MYO) protomer with

an energy penalty (positive) corresponding to the the difference in the protonation energies between the two protomers, ΔE_X^{prot}, (ii) the bioactive *non*-Pyri-H$^+$ (Pyri-H$^+$ for MYO) protomer of nicotinoid X is deformed from the gas phase geometry to assume its geometry in the pocket with an energy penalty (positive) of ΔE_X^{def}, (iii) the pocket is deformed from its gas phase geometry to assume its geometry when accommodating nicotinoid X with an energy penalty (positive) of $\Delta E_{p_i}^{def}$, (iv) the deformed bioactive *non*-Pyri-H$^+$ protomer (Pyri-H$^+$ for MYO) of nicotinoid X interacts with the deformed pocket with an interaction energy (negative) E_{int}. Therefore the total binding energy (negative) $\Delta E(X,\, p_i)$ of eq. (1) can be further decomposed into the following terms

$$\Delta E(X, p_i) = E_{int} + \Delta E_X^{prot} + \Delta E_X^{def} + \Delta E_{p_\mathrm{i}}^{def} \tag{2}$$

Additionally, we relied on the many-body expansion (MBE)[41–43] to identify important nicotinoid-peptide interactions and illustrate how such interactions change between nicotinoids. In the MBE, an observable (in this case the binding energy) is cast as the sum of many-body terms truncated to the third order

$$E_B = \sum_i E_{1\mathrm{B}_i} + \sum_{i,j} E_{2\mathrm{B}_{i,j}} + \sum_{i,j,k} E_{3\mathrm{B}_{i,j,k}} \tag{3}$$

where $E_{1\mathrm{B}_i}$ is the deformation energy of fragment i, $E_{2\mathrm{B}_{i,j}}$ is the pairwise interaction between fragments i and j, and $E_{3\mathrm{B}_{i,j,k}}$ is the non-pairwise additive interaction that emerges from the cooperative interaction between the three fragments i, j, and k. In equation 2, ΔE_X^{prot}, ΔE_X^{def}, $\Delta E_{p_\mathrm{i}}^{def}$, are parts of $\sum_i E_{1\mathrm{B}_i}$, and E_{int} is decomposed in the the mean $E_{2\mathrm{B}_{i,j}}$ and $E_{3\mathrm{B}_{i,j,k}}$. The terms in the MBE were compared across the different nicotinoids to identify the source of differences in the total binding.

The individual 2B components of the interaction energy were computed from *ab-initio*

calculations and compared with the ones obtained classically via

$$E_{\text{class}} = \sum_{i=1}^{N}\sum_{j=1}^{M} k\frac{q_i q_j}{r_{i,j}} + 4\epsilon_{i,j}\left(\left(\frac{\sigma_{i,j}}{r_{i,j}}\right)^{12} - \left(\frac{\sigma_{i,j}}{r_{i,j}}\right)^{6}\right) \tag{4}$$

where i and j index the atoms on each fragment, k is Coulomb's constant, q_i is the charge on atom i, $r_{i,j}$ is the distance between atoms i and j, and $\epsilon_{i,j}$ and $\sigma_{i,j}$ are parameters to describe the dispersion and Pauli-repulsion through a Lennard Jones type interaction. The charges q_i were determined from Natural Bond Order populations.[44] A single value of $\epsilon_{i,j}$ and $\sigma_{i,j}$ was used for each element for simplicity, derived from the most common values in the OPLS-AA force-field.[45] Hydrogens bound to electronegative atoms were assigned an ϵ value of zero, while hydrogens in the α position relative to the positive non-pyrrolidine nitrogen were assigned values of $\sigma = 0.500$, as in the OPLS3a force field.[46] The parameters used are provided in table S1.

III. Results and discussion

a. Binding of Nicotinoids to the Pocket

NIC binds to the nAChR model binding pockets similar to that reported in the crystal structures,[20,21] as indicated in figure 2 (e)-(f). The electronic energies of the components of eq. (1) are provided in table S2 of the Supporting Information (SI). The binding of the alkaloid to the pocket is mainly facilitated by a strong cationic hydrogen bonding interaction between the protic nitrogen and the carbonyl on residue Typ156, which is in agreement with NIC-nAChR interactions established in the crystal structure. Similar binding motifs are found for the other nicotinoids (figures S1-S3). For NOR, ANB, and ANT, the secondary protonated amine was forced to bind through the *cis*- hydrogen in a similar manner to NIC. Although binding through the *trans* hydrogen was lower in energy for the 3AA and 6AA model pockets, this structure was not found in the larger 14AA model pocket. Therefore,

only the *cis* binding is considered. COT binds similarly to NIC, while MYO deforms both itself and the pocket in order to bind, an efect that is caused by the surrounding steric residues in the larger model pockets.

The relative–to–NIC binding energies of the 5 other naturally occurring nicotinoids to the binding pockets was compared against their addictive thresholds in figure 4. These binding energies, listed in table 1, suggest that in general the less addictive nicotinoids bind less strongly with a higher (less negative) binding energy. The trend is strong and predictive for NIC, ANB, and NOR. In the 3AA model pocket, the correspondence between the binding energy and the ICSS threshold-increasing dosage is strong and predictive. In the 6AA model pocket the model incorrectly orders ANB and NOR. The 14AA model pocket predicts a more favorable binding for ANB than NIC, which is incosistant with their ICSS threshold-increasing dosages. Further investigations (*vide infra*) explain and rectify the orderings seen in the larger model pockets.

Table 1: The binding energies and the various components of equation 2 (kcal/mol) for the different nicotinoids interacting with the three model pockets.

Pocket (p_i)	Nicotinoid (X)	$\Delta E(X, p_i)$	ΔE_X^{prot}	ΔE_X^{def}	$\Delta E_{p_i}^{def}$	ΔE_{int}
3AA	NIC	-36.67	0.56	1.20	18.67	-57.10
	NOR	-33.20	5.28	0.96	18.68	-58.11
	ANB	-34.56	2.21	0.78	18.72	-56.26
	ANT	-39.80	3.20	1.07	19.14	-59.91
	MYO	-39.60	N/A	1.29	15.34	-59.53
	COT	-24.68	21.10	2.21	15.61	-63.60
6AA	NIC	-96.84	0.56	3.31	21.17	-121.88
	NOR	-92.16	5.28	2.94	21.18	-121.55
	ANB	-89.42	2.21	3.71	21.51	-116.85
	ANT	-88.49	3.20	2.22	19.92	-121.02
	MYO	-98.78	N/A	5.45	21.29	-118.33
	COT	-76.56	21.10	8.81	20.68	-127.16
14AA	NIC	-113.09	0.56	2.91	31.65	-148.22
	NOR	-109.47	5.28	1.86	35.82	-152.42
	ANB	-114.10	2.21	3.50	31.83	-151.64
	ANT	-112.48	3.20	4.03	32.09	-146.82
	MYO	-110.60	N/A	2.84	32.12	-150.54
	COT	-94.24	21.10	3.73	30.00	-149.07

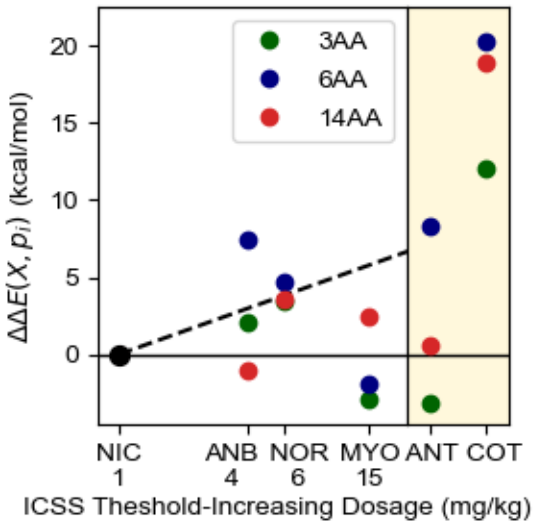

Figure 4: The binding energy (kcal/mol, relative to NIC) shown against the ICSS threshold-increasing dosages for the nicotinoids. In general, binding becomes less favorable for less addictive molecules. Nicotinoids in the yellow part of the figure are separated due to the lack of ICSS threshold-decreasing doses.

Not all nicotinoids clearly follow the trend produced by NIC, ANB NOR, and COT. From figure 4 it is seen that MYO binds more strongly than NIC in the smaller model pockets, despite being less addictive. Binding is a complex, multi-step process, involving dehydration, deformation, and interaction, while ion channel gating is an even more complicated process. To better understand the sources of the differences in the binding energies, and identify potentially useful descriptors of addictive thresholds, in the following we examine the individual contributions of the various components of equation 2 to the total binding.

b. Contribution of Monomer Deformation to the Binding Energy

The *non*-pyridine protomer (*non*-Pyri-H$^+$) is responsible for binding to the active nAChR. In the gas phase, this protomer is formed through proton transfer (ΔE_X^{prot}), except for MYO for which the *non*-Pyri-H$^+$ protomer is the gas phase global minimum. These proton exchange energies are plotted in figure 5. The same addictive trend previously observed for the binding energy (figure 4) is also observed for the monomer deformation piece for NIC,

NOR, and ANB, suggesting that the majority of the predictive trend in the proposed model may actually come from the proton exchange energies.

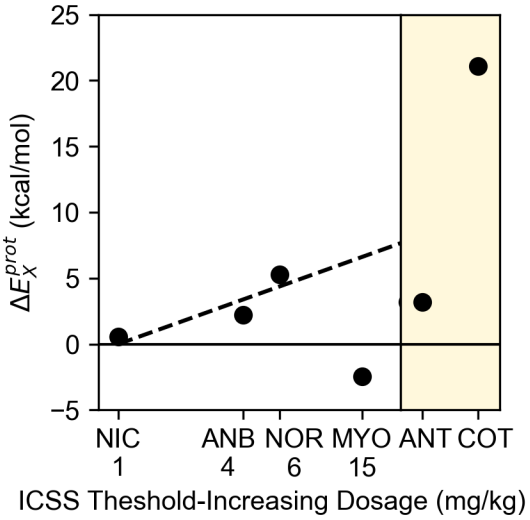

Figure 5: The proton exchange energy (energy difference between the H^+-Pyri and the *non*-Pyri-H^+ protomers) correlates with the ICSS threshold-increasing dosage of nicotinoids for the strongly addictive molecules.

It should be noted that in the real biological environment nicotinoids bind to the pocket in the human brain by moving from the aqueous state to the pocket (i.e., not from the gas phase to the pocket). The gas phase reference was chosen for this work for its simplicity, but a quick comparison to implicit solvent models was made to justify this choice. After all, the nicotinoids need to be desolvated in order to enter the pocket in the human brain as there is no water in the bound nicotinoid in the pocket. The desolvation energy of each nicotinoid was computed with PCM and is shown in figure S4. Although desolvation is not linearly related to proton exchange energy, the relationship is logarithmic and one-to-one. This shouldn't be surprising, as proton exchange energy and hydrogen bond strength are related to proton affinity.[47] Therefore, the same qualitative trend between binding energy and addiction can be produced with the reference being either the gas-phase H^+-Pyri or the aqueous state *non*-Pyri-H^+ protomers.

After assuming the local minima corresponding to *non*-Pyrro-H^+ protomers, the nicoti-

noids bind to the pocket. This process is naturally broken into two parts, deformation (for both the nicotinoid and the pocket) and interaction (between the deformed nicotoniod and the deformed pocket, see fig. 3), both of which influence the final geometries. The deformation energy (positive) is the energetic cost of moving from a local minimum to some deformed geometry of higher energy; the relative deformation energy (usually taken with respect to the NIC one) is the energy difference between deformed geometries. Although this energy contribution is important and sizable, there are no clear trends with addiction and the deformation energies of nicotinoids or pockets. Note that the pockets deform minimally to maximize interactions. These deformations are important, however, as small deformations in the protein can have a significant impact on the ability of the ion channel to open. Table S4 lists the root-mean-square-displacement (RMSD) in the structure of each amino acid referenced to the NIC-14AA structure. The largest structural differences are observed when MYO is bound to the pocket.

It was found that MYO had some of the largest deformations as it entered the binding pocket, mostly attributed to the change in the dihedral angle between the two rings, χ, defined in prior works.[23] For all the nicotinoids besides MYO, the minimum energy structures have χ angles near -7° (table S4). The conjugation in MYO naturally prefers a flattened structure with χ being -79°. The rotational landscapes of the nicotinoids are depicted in figure S5. The preferred angle χ for most nicotinoids inside the pocket exists between 0 and -30 degrees. MYO, however, must either deform strongly or relax into the pocket in some other way. It is found that MYO prefers the latter in the smaller pockets with deviations in the intermolecular degrees of freedom (figure S7). This is of serious concern since the mechanism of binding can have a significant impact on the activation of the receptor pore, which constitutes an important aspect of receptor activation and the addiction mechanism.

c. Interactions with Amino Acids

The final but arguably more complicated aspect of binding is the interaction of the ligand and the receptor (E_{int}). This interaction can be viewed through fragment many-body energies, a direct consequence of the respective intermolecular geometry. All of these will be utilized in this section to understand more fundamentally how nicotinoids interact with the binding pocket of nAChRs as well as illuminate how different aspects of this binding support the addictive aspects of these molecules.

A beneficial consequence of the approach of fragmented model pockets used in this study is that the MBE naturally allows for the ability to separate distinct nicotinoid-peptide interactions. Arguably, one of the most important interactions included in all model pockets is the interaction between the nicotinoid and TYP 156; since TYP 156 is modeled as a polypeptide chain, this fragment will be called α156. This is a strong interaction (between -43.69 and -59.51 kcal/mol, values reported in table S5) coming from a charged hydrogen bond, cation-pi interactions, and additional van-der-Waals interactions. Subtle differences in this pairwise interaction energy penalize nicotinoids ANB, ANT, and MYO, shown by the positive bars in figure 6. This interaction is dominated by the cationic hydrogen bond between the nicotinoid and Typ 156, as indicated by the correlation between the α156-nicotinoid two body energy and the elongation of the C-O carbonyl in Typ156, the hydrogen bond acceptor (Figure 6). Deviations from this correlation occur naturally through non-hydrogen bonding interactions. Unsurprisingly, COT forms the strongest hydrogen bond, as it is the most acidic. The hydrogen bonds are stronger in the 6AA model than the 3AA model, a direct consequence of the increased nucleophilicity of α156 chained and a tighter bound geometry to the Asp96 residue. This increased nucleophilicity manifests not only in the Trp156 residue, but all residues on this polypeptide, including Ser155.

Another conserved interaction is that between the nicotinoid and the Typβ57 residue (Figure 7). It is strongly favorable in ANT, MYO and COT for the 3AA model, likely resulting from slight conformational changes decreasing H-π distances due to the missing

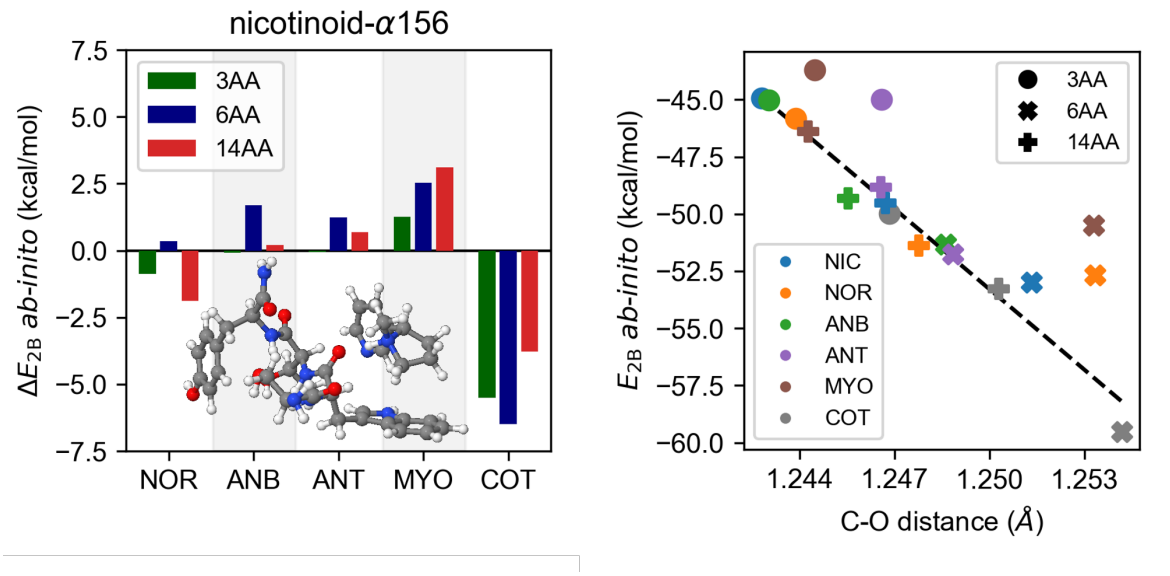

Figure 6: Left panel: the two body energy for the nicotinoid-α156 chain relative to that of NIC is plotted for the various nicotinoids and model pockets. Right panel: the attractive (negative) two body energies are plotted against a metric of the length of the carbonyl in the Typ156 residue, which constitutes a metric of hydrogen bond strength.

steric hindrance. As additional amino acid residues are added in the larger pockets, the interaction becomes continually less favorable, and consistently less favorable than NIC for NOR, ANB, ANT, and MYO. The RMSD of the Typβ57 residue (table S3) shows that the closer geometry comes mostly from changes in the position of the residue.

As discussed earlier, the additional amino acid residues in the 6AA model change the way nicotiniods interact with the α156 residue and the β57 residue. These interactions do not, however, have marked differences between nicotinoids; plots of these interactions are supplied in figure S6. It becomes more important to discuss how the increasing nucleophilicity changes the structure of the nicotinoids in the pocket. The coordinates to describe the orientational changes of the nicotinoids between pocket models are described in figure S7. The increased nucleophilicity of the pocket results in the change (bending) of the orientation of the nicotinoids, specifically moving the nicotinoid closer to the c-terminus of the α156 chain. This is a manifestation of the Typ156's increased nucleophilicity making the hydrogen bond to the carbonyl closer to 120° and stronger. This bending also adds a slightly favorable

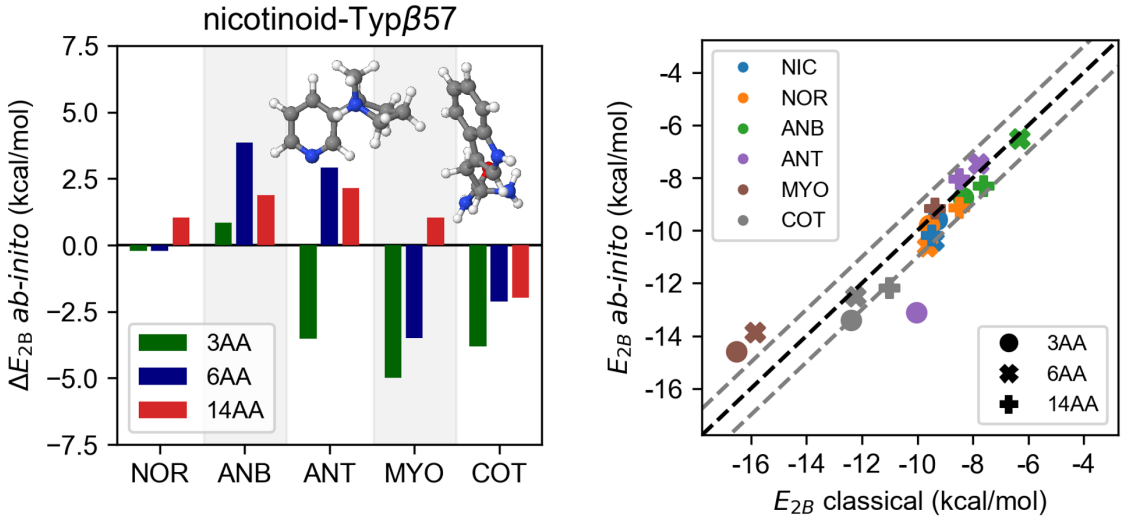

Figure 7: Left panel: the two body energies for the nicotinoid-Typβ57 residue relative to that of NIC is plotted for the various nicotinoids. Right panel: Correlation between the *ab-initio* and classical energies, indicating that these interactions are largely classical. Gray lines indicate an error of 1 kcal/mol.

C-H hydrogen bond with the Ser155 residue and affects the ANB and ANT less favorably due to the larger 6-membered rings having larger steric interactions with neighboring residues. Steric interactions in the 14AA model return most orientations to those observed in the 3AA model. Therefore, the structures and subsequent energies computed in the 6AA model maybe an artifact of the geometries assumed in the smaller pockets compared to that of the full protein.

Amino acids in the 14AA model similarly change the way nicotinoids interact with the α156 chain as discussed earlier. Some have large contributions to the relative binding energy and will be discussed here. Nicotinoids form weak CH$\cdots$O interactions between the N-α carbon atoms and the hydroxide of the Tyr100 residue, see figure 9. This interaction is maximized in NIC by two N-α hydrogen atoms. In contrast, NOR, ANB, ANT, and MYO have only one N-α hydrogen atom so this interaction is consistently less favorable. On the other hand, the interactions of COT are distant and weak due to the additional carbonyl. Another residue, Tyr204, interacts with protonated secondary amines in favorable ways that

strongly impact the relative binding energy (figure 8). In NIC and COT, this residue accepts a weak CH$\cdots\pi$ bond between the methyl group and the phenol group. In NOR, ANB, and ANT, the methyl group is replaced by hydrogen, which forms a second protonated hydrogen bond. Leuβ104 has stronger interactions with MYO than with other nicotinoids (figure 10). We attribute this result to the higher multi-pole moment on the pyridine ring of MYO due to larger partial positive and negative charges on the atoms, see table S6, which comes from the conjugation of the pyridine ring to the protonated nitrogen on the five-membered ring. This increased multipole moment also appears as an increased electrostatic interaction when modeled via pairwise point charges. Leuβ104 has comparable dimer energies with the other nicotinoids and the remaining amino acid residues interact similarly with the set of nicotinoids. Other nicotinoid-peptide interactions are supplied in figures S8-S9 for reference.

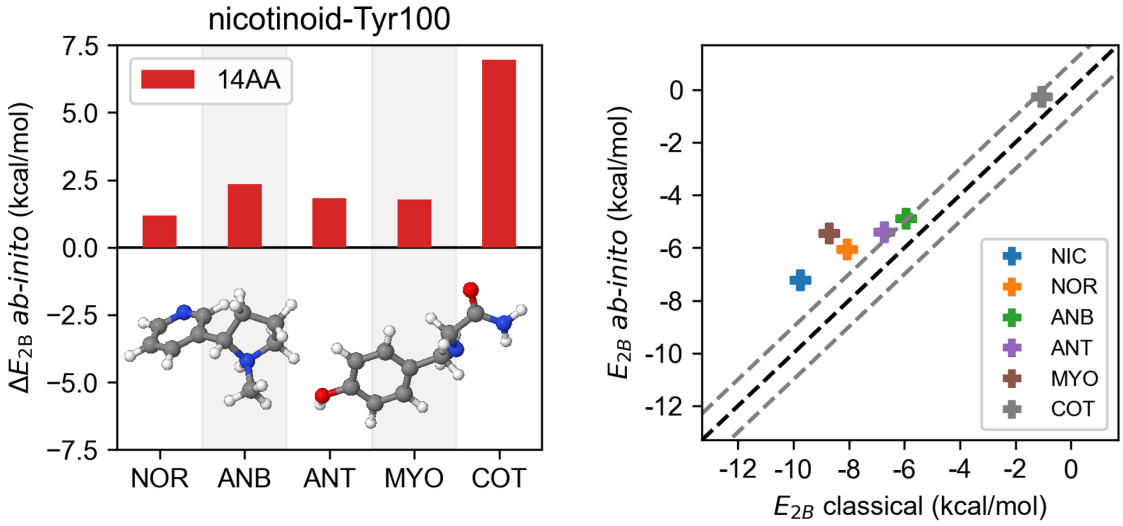

Figure 8: Left panel: the two body energy for the nicotinoid-Tyr100 residue relative to that of NIC shown for the various nicotinoids. Right panel: Correlation between the *ab-initio* and classical energies, indicating that these interactions are largely classical. Gray lines indicate an error of 1 kcal/mol.

The relative-to-NIC 2B energies are shown in the left panel of figure 11, whereas the relative-to-NIC 3B energies are plotted in the right panel of tht figure. In general, two-body energies (E_{2B}) between peptides are small and near equivalent regardless of the identity of

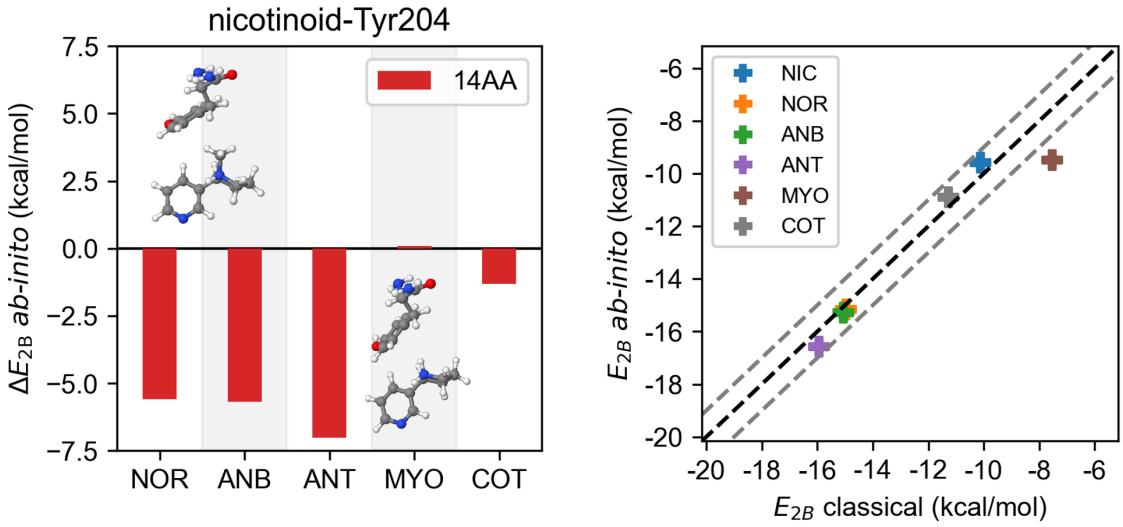

Figure 9: Left panel: the two body energy for the nicotinoid-Tyr204 residue relative to that of NIC shown for the various nicotinoids. Right panel: Correlation between the *ab-initio* and classical energies, indicating that these interactions are largely classical. Gray lines indicate an error of 1 kcal/mol

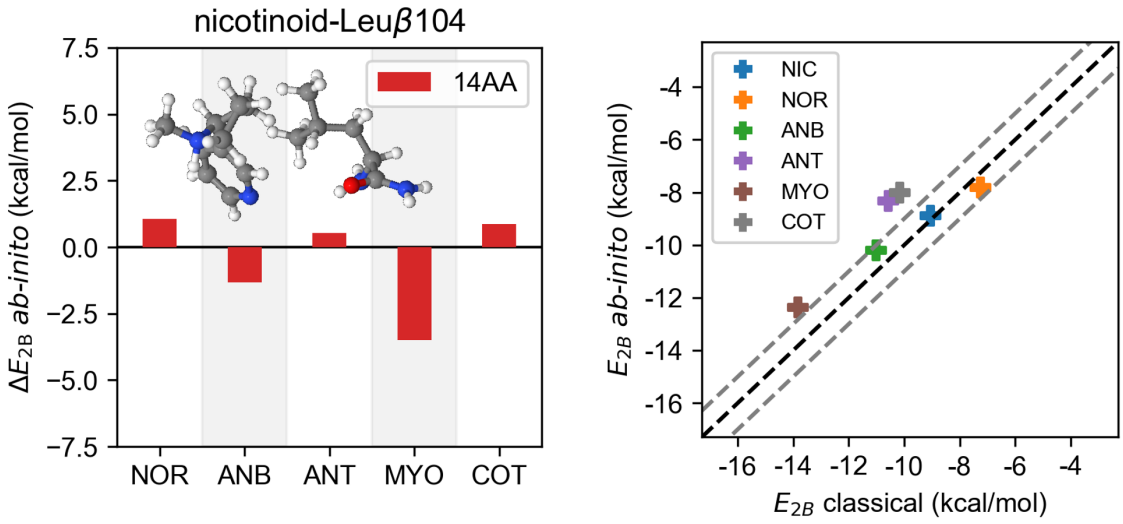

Figure 10: Left panel: the two body energy for the nicotinoid-Tyr204 residue relative to that of NIC shown for the various nicotinoids. Right panel: Correlation between the *ab-initio* and classical energies, indicating that these interactions are largely classical. Gray lines indicate an error of 1 kcal/mol

the nicotinoid in the pocket. In addition, differences in peptide-peptide 2B energies in the presence of different nicotinoids are small, as shown by the visible blue sections centered around zero. The average value for these relative-to-NIC peptide-peptide 2B energies is 0.0094 kcal/mol with a standard deviation of 0.82 kcal/mol. A few terms are large in magnitude and will be discussed later.

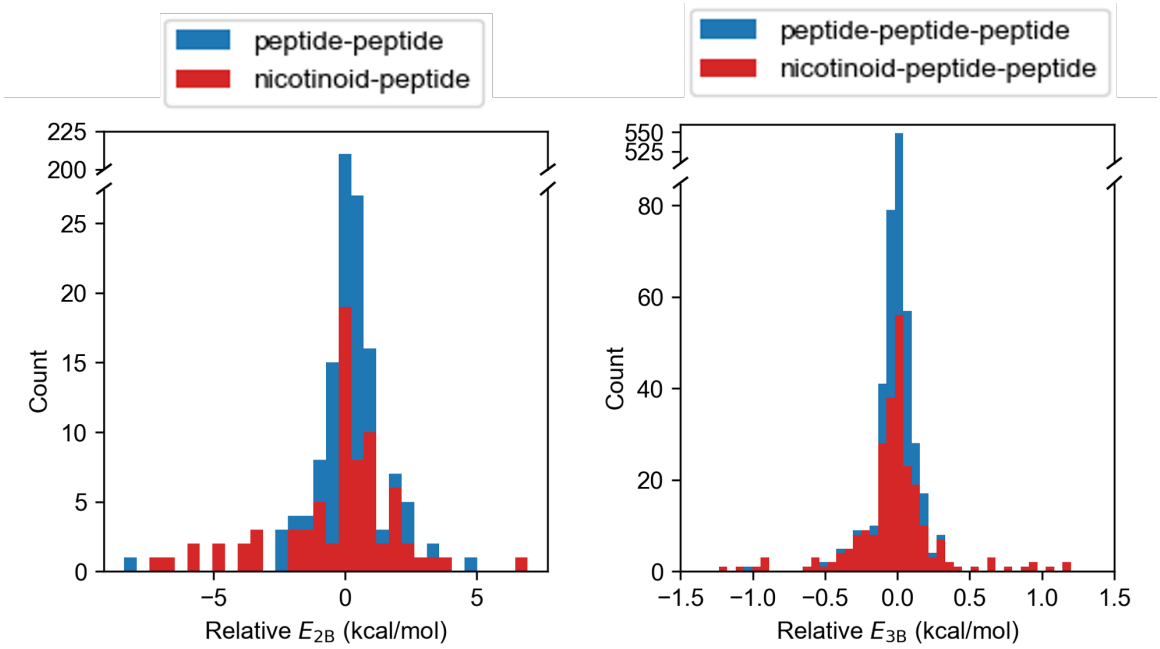

Figure 11: All two- and three-body terms, relative to those of nicotine, shown as histograms on the left and right panels, respectively. Red colors denote nicotinoid-peptide, whereas blue colors denote those between peptides and are stacked above the red ones. Note the breaks near the top of the y-axis.

Exceptions arise only for NOR and MYO, specifically for dimers SERβ108-α156, SERβ108-LEUβ104, TYR 197-TYR204, TYR204-α156, TYR204-ASP96, TYR204-α156, and TYR204-Cys199:200. Most 2B interactions pair up and cancel, such as the SERβ108-α156 and SERβ108-LEUβ104, which cancel each other. The energetic differences can be attributed to a rotation of the hydroxyl group trading dipole-induced dipole interactions with the α156 chain for distant dipole-dipole interaction with the Leuβ104 carbonyl. A similar hydroxyl rotation pairs the Tyr204-Tyr197 and Tyr204-Asp96 residues. Interactions do not fully cancel for Tyr204-α156 and Try204-Cys199:200 when MYO is bound to the pocket. Significant

conformational changes (see table S3) in the Tyr204 residue increase favorable interactions with α156, while breaking favorable interactions with the C-Loop domain. This is of serious concern in the closing of the pocket by the C-Loop.

The interactions of nicotinoids with Tyr204 are of interest because they were shown to interact differently with neighboring residues depending on the identity of the nicotinoid added to the pocket. This residue forms strong hydrogen bonding interactions with NOR, ANB, and ANT and the orientational changes alter the interactions of this residue with the Cystines of the C-Loop domain. This interaction region is important for the activation process. Additionally, Tyr204 is suspected to interact with a water molecule that is present in the acetylcholine-binding protein (AChBP). The water molecule is not included in the present work, which models the interaction of nicotinoids with the acetylcholine receptor (nAChR), where there is no water present. Although numerous past studies found a water molecule forming hydrogen bonds between TYR240, SERβ108, and NIC in AChBPs and other variants of nAChRs,,[16,17,19] the crystal structure by Morales et.al and Walsh et.al. does not detect a water molecule at this site.[20,21] For this reason water was not added to the pocket. The changes made by NOR and MYO to the Tyr204 residue would disrupt the interactions with water. Further exploration, either computational or experimental, is warranted to confirm the absence or presence of water in the $\alpha_4\beta_2$ variant of the nAChR.

Three-body energies (E_{3B}) are consistently small and near equivalent. The relative-to-NIC 3B energies are plotted in the right panel of figure 11. None of these are large in magnitude and most are near zero; their average value of relative-to-NIC 3B energies is -0.0017 kcal/mol with a standard deviation of 0.17 kcal/mol. Even the absolute 3B energy terms are negligible and centered around zero (figure S10); their average value is 0.011 kcal/mol with a standard deviation of 1.22 kcal/mol. The only large 3B terms belong to the nicotinoid-α156-Asp96 trimer. The corresponding dimers also contribute to large 2B terms (figure S10).

d. Piecemeal Steps of Binding Provide a Predictive Model

The analysis of nicotinoid-peptide interactions with select amino acid residues provides a unique opportunity to develop a model for predicting addiction of nicotinoids. Trends in proton exchange energy support the notion that simplistic, one-body effects can describe the ability for a nicotinoid to elicit changes in ICSS threshold and be addictive. Deviations from this trend are rectified via peptide-nicotinoid interactions, most importantly between the nicotinoid and the amino acid residues in its immediate vicinity. Figure 12 shows the trends when considering only a subset of interactions in each model. The upper left panel includes all one-body terms, viz. proton exchange, nicotinoid deformation, and peptide (pocket) deformation. The upper right panel incorporates all 2- and 3-body effects between the nicotinoid, the α156 chain, and the Typβ57 residue. The lower left panel includes the 2- and 3-body interactions that include the nicotinoid, the α156 chain, the Typβ57, and the Asp97 residues. Finally, the bottom right panel includes all prior and all 2-body interactions between the additional peptides in the 14AA model except for all Tyr204 interaction and the Leuβ104-nicotinoid interaction. The Tyr204 amino acid is excluded due to the deformations and interactions that have the potential to change the tertiary structure of the C-Loop region. The Leuβ104-nicotinoid was removed due to the strong quadrupole-quadrupole interaction between the LEUβ104 and MYO, which changes the orientation of the pyridine ring in MYO and may disrupt the speculative interaction with a water molecule (when present).

When taking into account only the nicotinoid and peptide deformations, a reasonable predictive relationship is established for the 14AA model. Steric type interactions, that restrict the ways MYO relaxes into the pocket appear to capture the relative unfavorable binding of MYO to the nAChR. The interactions of nicotinods with local binding residues further diminish MYO's binding, therefore explaining its low addicitve ability. In the simpler models (smaller pockets), NOR's quite relatively favorable binding to the α156 chain results in a lower binding energy than ANB. Incorporating the interactions of the nicoinoids and other amino acid residues prove to be important in predicting the order of ICSS threshold-

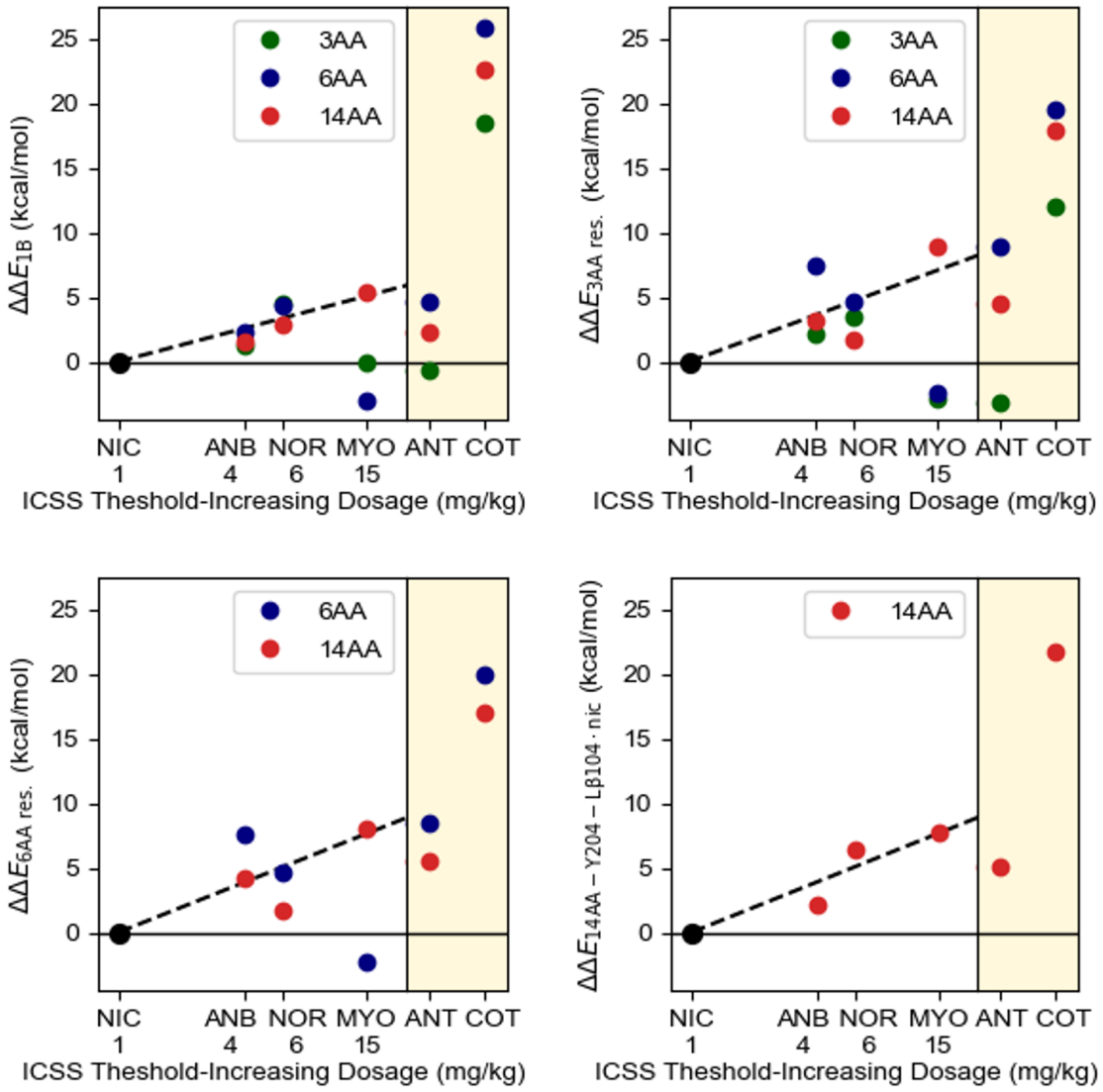

Figure 12: The ICSS threshold-increasing dosages are compared against the sum of certain binding terms, viz. one body terms (upper left), terms involving only fragments in the 3AA model (upper right), terms involving fragments in the 6AA model (lower left), and all terms except for those involving Tyr204 and Leuβ104-nicotinoid interactions (lower right).

increasing dosages. Interactions and their differences are small (<5 and <1 kcal/mol respectively), however numerous. The reduced summation of the 14AA model, in which the Tyr204 interactions and the Leuβ104-nicotinoid interaction were eliminated, proves to be sufficient in predicting ICSS threshold-increasing doses. It serves as a good descriptor for predicting the psychoactive character and resulting addictive potential of nicotinoids. Caution should be taken, however, in ensuring that large changes are not observed with a test nicotinoid that is structurally different from nicotine and may change the structure of the nAChR in ways not observed in this work.

IV. Conclusions

The binding energy of nicotinoids with the amino acid residues of the $\alpha_4\beta_2$ variant of the nAChR has proven to be an invaluable descriptor in predicting the addictive character of nicotine-like molecules. In general, nicotinoids that bind more strongly to the peptides are more addictive. The source of differences in binding spans intrinsic nicotinoid descriptors, such as proton affinity/proton exchange and to peptide-nicotinoid interactions.

The model pockets of increasing sizes, derived from the crystal structure of the nAChR, accurately describe the relative interactions of the guest nicotinoids to the host nAChR environment. Differences in the total interaction originate mainly from pairwise, two-body terms. Non-additive (3B) interactions are generally small, with the differences of these terms between nicotinoids being even smaller. Although many amino acids interact similarly with all nicotinoids, most of the differences arise in the restriction of the configuration space of the nicotinoid and therefore, its interactions with important residues such as TYP156 and TYPβ57. The pairwise interactions between the nicotinoids and distant amino acids (such as those present in the 14AA model) can be accurately described by simpler, lower scaling classical force fields. However, the interactions of nicotinoids with proximal amino acids (such as the α156 chain and Asp96 residues) should remain modeled by quantum

mechanical methods.

Evidence presented in this work supports future investigations into the possibility of the presence of water in the binding pocket. Although water was not detected in the X-ray structure by Morales et.al.,[20,21] there exist both hydrogen bond donors and acceptors spaced appropriately for water to bind in the pocket. The presence of a single water molecule would greatly impact the positioning of NOR and MYO in the pocket and thus affect the interactions of the nicotinoid with the Tyr204, Leuβ104 and Serβ108 residues. Further investigations and simulations including a single water molecule will serve to modify these interactions and explain the potential role that water can have in the binding mechanism.

Acknowledgement

We thank Prof. Andrew Harris of the University of Minnesota for providing the raw data of Reference[3] that was used to construct Figure 1. GDS and SSX were supported by U.S. Department of Energy (DOE), Office of Science, Office of Basic Energy Sciences, Division of Chemical Sciences, Geosciences, and Biosciences, Condensed Phase and Interfacial Molecular Science (CPIMS) program, Molecular Theory and Modeling FWP 16249 at Pacific Northwest National Laboratory (PNNL), a multi-program national laboratory operated for DOE by Battelle. This research also used resources of the National Energy Research Scientific Computing Center, which is supported by the Office of Science of the U.S. Department of Energy under Contract No. DE-AC02-05CH11231. YO, KH, SI and MF were supported in part by KAKENHI (JP18H01938, JP19H05527, JP19K23624, JP20H00372) and the Core-to-core program (JPJSCCA20210004) of JSPS, World Research Hub Initiative in the Tokyo Institute of Technology, the Cooperative Research Program of the "Network Joint Research Center for Materials and Devices" from the Ministry of Education, Culture, Sports, Science and Technology (MEXT), Japan, and the RIKEN Pioneering Project, "Fundamental Principles Underlying the Hierarchy of Matter: A Comprehensive Experimental Study".

Supporting Information Available

The following files are available free of charge.

- Supporting Information.pdf: Additional figures and figures to supplement claims in the paper. Cartesian geometries of nicotinoids and pockets are provided.

References

(1) Griffiths, R. R.; Bigelow, G. E.; Liebson, I. Facilitation of Human Tobacco Self-Administration by Ethanol: A Behavioral Analysis. *J. Exp. Anal. Behav.* **1976**, *25*, 279–292.

(2) Benowitz, N. L. Pharmacology of Nicotine: Addiction, Smoking-Induced Disease, and Therapeutics. *Annu. Rev. Pharmacol. Toxicol.* **2009**, *49*, 57–71.

(3) Harris, A. C.; Tally, L.; Muelken, P.; Banal, A.; Schmidt, C. E.; Cao, Q.; LeSage, M. G. Effects of nicotine and minor tobacco alkaloids on intracranial-self-stimulation in rats. *Drug Alcohol Depend.* **2015**, *153*, 330–334.

(4) US Food and Drug Administation. *Results from the Annual National Youth Tobacco Survey* . `https://www.fda.gov/tobacco-products/public-health-education/youth- and-tobacco` (accessed 2023-10-19).

(5) U.S. Department of Health and Human Services. Patterns of E-Cigarette Use Among U.S. Youth and Young Adults. In *E-Cigarette Use Among Youth and Young Adults: A Report of the Surgeon General*. U.S. Department of Health and Human Services, Centers for Disease Control and Prevention, National Center for Chronic Disease Prevention and Health Promotion: Atlanta, GA, Office on Smoking and Health, 2016; 27-89.

(6) Federal Register. *Tobacco Product Standard for Nicotine Level of Combusted Cigarettes*. `https://www.federalregister.gov/documents/2018/03/16/2018-05345/tobacco- product-standard-for-nicotine-level-of-combusted-cigarettes` (accessed 2023- 10-19).

(7) US Food and Drug Administation. *FDA Announces Plans for Proposed Rule to Reduce*

Addictiveness of Cigarettes and Other Combusted Tobacco Products. https://www.fda.gov/news-events/press-announcements/fda-announces-plans-proposed-rule-reduce-addictiveness-cigarettes-and-other-combusted-tobacco (accessed 2023- 10-19).

(8) Papke, R. L.; Dwoskin, L. P.; Crooks, P. A. The pharmacological activity of nicotine and nornicotine on nAChRs subtypes: relevance to nicotine dependence and drug discovery. *J. Neurochem.* **2007**, *101*, 160–167.

(9) Dani, J. A.; De Biasi, M. Cellular mechanisms of nicotine addiction. *Pharmacol. Biochem. Behav.* **2001**, *70*, 439–446, The Psychopharmacology of Nicotine.

(10) Dani, J. A. In *Nicotine Use in Mental Illness and Neurological Disorders*; De Biasi, M., Ed.; Int. Rev. Neurobiol.; Academic Press, 2015; Vol. 124; pp 3–19.

(11) Ma, K.-G.; Qian, Y.-H. Alpha 7 nicotinic acetylcholine receptor and its effects on Alzheimer's disease. *Neuropeptides* **2019**, *73*, 96–106.

(12) Tregellas, J. R.; Wylie, K. P. Alpha7 Nicotinic Receptors as Therapeutic Targets in Schizophrenia. *Nicotine Tobacco Research* **2018**, *21*, 349–356.

(13) Freedman, R. α7-Nicotinic Acetylcholine Receptor Agonists for Cognitive Enhancement in Schizophrenia. *Annu. Rev. Med.* **2014**, *65*, 245–261.

(14) Hogg, R. C.; Rassenbass, M.; Bertrand, D. Nicotinic acetylcholine receptors: from structure to brain function. *Rev. Physiol. Biochem. Pharmacol.* **2003**, *147*, 1–46.

(15) Unwin, N.; Fujiyoshi, Y. Gating Movement of Acetylcholine Receptor Caught by Plunge-Freezing. *J. Mol. Biol.* **2012**, *422*, 617–634.

(16) Amiri, S.; Sansom, M. S.; Biggin, P. C. Molecular dynamics studies of AChBP with nicotine and carbamylcholine: the role of water in the binding pocket. *Protein Eng. Des. Sel.* **2007**, *20*, 353–359.

(17) Brejc, K.; van Dijk, W. J.; Klaassen, R. V.; Schuurmans, M.; van der Oost, J.; B., S. A.; Sixma, T. K. Crystal structure of an ACh-binding protein reveals the ligand-binding domain of nicotinic receptors. *Nature* **2001**, *411*, 269–276.

(18) Zhao, Y.; Liu, S.; Zhou, Y.; Zhang, M.; Chen, H.; Xu, H. E.; Sun, D.; Liu, L.; Tian, C. Structural basis of human α7 nicotinic acetylcholine receptor activation. *Cell Res.* **2021**, *31*, 713–716.

(19) Gharpure, A.; Teng, J.; Zhuang, Y.; Noviello, C. M.; Walsh, R. M.; Cabuco, R.; Howard, R. J.; Zaveri, N. T.; Lindahl, E.; Hibbs, R. E. Agonist Selectivity and Ion Permeation in the $\alpha 3\beta 4$ Ganglionic Nicotinic Receptor. *Neuron* **2019**, *104*, 501–511.e6.

(20) Morales-Perez, C. L.; Noviello, C. M.; Hibbs, R. E. X-ray structure of the human $\alpha 4\beta 2$ nicotinic receptor. *Nature* **2016**, *538*, 411–415.

(21) Walsh Jr., R. M.; Roh, S.-H.; Gharpure, A.; Morales-Perez, C. L.; Ryan E. Hibbs, J. T. Structural principles of distinct assemblies of the human $\alpha 4\beta 2$ nicotinic receptor. *Nature* **2018**, *557*, 261–265.

(22) Graton, J.; Berthelot, M.; Gal, J.-F.; Girard, S.; Laurence, C.; Lebreton, J.; Le Questel, J.-Y.; Maria, P.-C.; Nauš, P. Site of Protonation of Nicotine and Nornicotine in the Gas Phase: Pyridine or Pyrrolidine Nitrogen? *J. Am. Chem. Soc.* **2002**, *124*, 10552–10562.

(23) Yoshida, T.; Farone, W. A.; Xantheas, S. S. Isomers and Conformational Barriers

of Gas-Phase Nicotine, Nornicotine, and Their Protonated Forms. *J. Chem. Phys. B* **2014**, *118*, 8273–8285.

(24) Santis, G. D.; Takeda, N.; Hirata, K.; Tsuruta, K.; Ishiuchi, S.-i.; Xantheas, S. S.; Fujii, M. Structure of Gas Phase Monohydrated Nicotine: Implications for Nicotine's Native Structure in the Acetylcholine Binding Protein. *J. Am. Chem. Soc.* **2022**, *144*, 16698–16702.

(25) Clayton, P. M.; Vas, C. A.; Bui, T. T. T.; Drake, A. F.; McAdam, K. Spectroscopic investigations into the acid–base properties of nicotine at different temperatures. *Anal. Methods* **2013**, *5*, 81–88.

(26) Linnell, R. H. Anabasine. *J. Am. Chem. Soc.* **1954**, *76*, 1391–1393.

(27) Chen, B.; Xu, Q. Protonating and determining myosmine intactly by association with citrate anion. *Analyst* **2011**, *136*, 4846–4854.

(28) Takeda, N.; Hirata, K.; Tsuruta, K.; Santis, G. D.; Xantheas, S. S.; Ishiuchi, S.-i.; Fujii, M. Gas phase protonated nicotine is a mixture of pyridine- and pyrrolidine-protonated conformers: implications for its native structure in the nicotinic acetylcholine receptor. *Phys. Chem. Chem. Phys.* **2022**, *24*, 5786–5793.

(29) Chai, J.-D.; Head-Gordon, M. Long-range corrected hybrid density functionals with damped atom–atom dispersion corrections. *Phys. Chem. Chem. Phys.* **2008**, *10*, 6615–6620.

(30) Francl, M. M.; Pietro, W. J.; Hehre, W. J.; Binkley, J. S.; Gordon, M. S.; DeFrees, D. J.; Pople, J. A. Self-consistent molecular orbital methods. XXIII. A polarization-type basis set for second-row elements. *J. Chem. Phys.* **1982**, *77*, 3654–3665.

(31) Hariharan, P. C.; Pople, J. A. The influence of polarization functions on molecular orbital hydrogenation energies. *Theoret. Chim. Acta* **1973**, *28*, 213–222.

(32) Kohn, W.; Becke, A. D.; Parr, R. G. Density Functional Theory of Electronic Structure. *J. Chem. Phys.* **1996**, *100*, 12974–12980.

(33) Frisch, M. J. et al. Gaussian˜16 Revision C.01. 2016; Gaussian Inc. Wallingford CT.

(34) Gordon, M. S.; Binkley, J. S.; Pople, J. A.; Pietro, W. J.; Hehre, W. J. Self-consistent molecular-orbital methods. 22. Small split-valence basis sets for second-row elements. *J. Am. Chem. Soc.* **1982**, *104*, 2797–2803.

(35) Clark, T.; Chandrasekhar, J.; Spitznagel, G. W.; Schleyer, P. V. R. Efficient diffuse function-augmented basis sets for anion calculations. III. The 3-21+G basis set for first-row elements, Li–F. *J Comput Chem* **1983**, *4*, 294–301.

(36) Tomasi, J.; Mennucci, B.; Cammi, R. Quantum Mechanical Continuum Solvation Models. *Chem. Rev.* **2005**, *105*, 2999–3094.

(37) Remya, K.; Suresh, C. H. Which density functional is close to CCSD accuracy to describe geometry and interaction energy of small noncovalent dimers? A benchmark study using Gaussian09. *J Comput Chem* **2013**, *34*, 1341–1353.

(38) Herman, K. M.; Aprà, E.; Xantheas, S. S. A critical comparison of CH versus interactions in the benzene dimer: obtaining benchmarks at the CCSD(T) level and assessing the accuracy of lower scaling methods. *Phys. Chem. Chem. Phys.* **2023**, *25*, 4824–4838.

(39) Morales-Perez, C. L.; Noviello, C.M.; Hibbs, R. E. X-ray structure of the human $\alpha 4\beta 2$ nicotnic receptor, (2016), `https://doi.org/10.2210/pdb5KXI/pdb`.

(40) Negus, S. S.; Miller, L. L.; Nader, M. A. Intracranial Self-Stimulation to Evaluate Abuse Potential of Drugs. *Pharmacol. Rev.* **2014**, *66*, 869–917.

(41) Roberts, F.; Tesman, B. U. *Applied Combinatorics*, 2nd ed.; Taylor Francis: New York, 2009.

(42) Hankins, D.; Moskowitz, J. W.; Stillinger, F. H. Water Molecule Interactions. *J. Chem. Phys.* **2003**, *53*, 4544–4554.

(43) Xantheas, S. S. Ab initio studies of cyclic water clusters $(H_2O)_n$, n=1–6. II. Analysis of many-body interactions. *J. Chem. Phys.* **1994**, *100*, 7523–7534.

(44) Reed, A. E.; Weinstock, R. B.; Weinhold, F. Natural Population Analysis. *J. Chem. Phys.* **1985**, *83*, 735–746.

(45) Jorgensen, W. L.; Maxwell, D. S.; Tirado-Rives, J. Development and Testing of the OPLS All-Atom Force Field on Conformational Energetics and Properties of Organic Liquids. *J. Am. Chem. Soc.* **1996**, *118*, 11225–11236.

(46) Roos, K.; Wu, C.; Damm, W.; Reboul, M.; Stevenson, J. M.; Lu, C.; Dahlgren, M. K.; Mondal, S.; Chen, W.; Wang, L.; Abel, R.; Friesner, R. A.; Harder, E. D. OPLS3e: Extending Force Field Coverage for Drug-Like Small Molecules. *J. Chem. Theory Comput.* **2019**, *15*, 1863–1874.

(47) Mautner, M. The ionic hydrogen bond and ion solvation. 1. $NH^+\cdots O$, $NH^+\cdots N$, and $OH^+\cdots O$ bonds. Correlations with proton affinity. Deviations due to structural effects. *J. Am. Chem. Soc.* **1984**, *106*, 1257–1264.

TOC Graphic